Simple accurate model of silicon donor arrays

Chao Lei and Allan H. MacDonald
Department of Physics, University of Texas, Austin, Texas 78712, USA

(Received 20 May 2021; revised 15 May 2022; accepted 14 July 2022; published 25 July 2022)

Donors in silicon can now be positioned with an accuracy of about one lattice constant, making it possible to form donor arrays for quantum computation or quantum simulation applications. However, the multivalley character of the silicon conduction band combines with central cell corrections to the donor states to convert small atomic scale imperfections in donor placement into strong interdonor hybridization disorder. We present a simple model that is able to account for central cell corrections accurately, and use it to assess the impact of donor positional disorder on donor array properties in both itinerant and localized limits. Our results show that donor arrays in silicon simulate strongly disordered one-dimensional electrons.

DOI: 10.1103/PhysRevB.106.045305

I. INTRODUCTION

One strategy for establishing robust solid state quantum information processing hardware is to exploit the relatively simple bound states that surround donors or acceptors in the best understood semiconductor material, silicon [1,2]. Considerable experimental progress has been made toward the use the electron spin of a donor bound state in silicon, or alternately the donor nuclear spin, as a qubit [3–20]. It has been possible, for example, to achieve long coherence times for both electron [21,22] and nuclear spins [23]. Additionally, advances in the technology for deterministically implanting donors in silicon [24–28] with high positional accuracy have made it possible to form donor arrays [illustrated in Fig. 1(a)], which are attractive for both quantum computation [29] and quantum simulation [24,30,31] applications. However, the physics of donor arrays in silicon is complicated by the presence of six valleys in the silicon conduction band, which adds an unwanted valley degree of freedom to donor bound electron envelope function Hamiltonians. The valley degeneracy is lifted by central cell corrections that couple valleys [32,33]. There is still an unwanted complication, however, since mixing between valleys makes the interactions between donor levels extremely sensitive to donor positional disorder, as we will discuss in this paper. Even the lattice constant scale accuracy in donor positioning now achievable in a silicon crystal [34] is not necessarily adequate.

To describe this physics, we introduce a model for the central cell interactions that are responsible for the valley splitting of donor levels in bulk silicon. The model is attractively simple and captures all the essential multivalley physics. We use it to assess the effectiveness of recently proposed strategies [35,36] to mitigate the influence of positional disorder on the exchange coupling between two spin qubits in the localized limit, demonstrating that they are less sensitive to positional disorder when oriented along $\langle 110\rangle$ rather than along $\langle 100\rangle$. In the itinerant limit, positional disorder localizes donor array Bloch states. We show that this effect is also strongly limited by placing the donor array along $\langle 110\rangle$. Our calculations demonstrate that central cell corrections which separate the A_1 bound state [Fig. 1(c)] from other disorder levels play a central role in determining donor array properties in both localized and itinerant limits.

II. PERIODIC ARRAY OF DONORS

Donors in silicon have been well understood for decades [37–42]. The donor levels are located in the semiconductor gap, close to the bottom of the conduction band as illustrated in Fig. 1(b). To estimate the binding energies relative to the bottom of the conduction band, we employ an effective mass approach [37,38] in which the wave function of an electron bound to an isolated donor has the form

$$\psi(\mathbf{r}) = \sum_{\mu=1}^{N_\mu} F_\mu(\mathbf{r})\phi_\mu(\mathbf{r}), \tag{1}$$

where μ labels valley, $N_\mu = 6$ is the number of valleys, $F_\mu(\mathbf{r})$ is an envelope function, and $\phi_\mu(\mathbf{r}) = e^{i\mathbf{k}\cdot\mathbf{r}}u_\mu(\mathbf{r})$ is a band minimum Bloch function with periodic factor $u_\mu(\mathbf{r})$.

When central cell corrections are neglected there is no coupling between valleys, and donor bound states in each valley are eigenstates of an effective mass Schrödinger equation [38] with Hamiltonian

$$H = \sum_i \frac{\hbar^2}{2m_i^*}\nabla_i^2 + V(\mathbf{r}). \tag{2}$$

Here $i = x, y, z$, m_i are effective masses, and $V(\mathbf{r}) = -e^2/\epsilon|\mathbf{r}|^2$ is the hydrogenic external potential induced by the replacement of a Si atom by a donor ion at the origin. The mass tensor in Eq. (2) is diagonal because the six conduction band valleys in silicon are located along the principle cubic axes, with a large mass m_i for momentum along the valley direction (longitudinal mass $m_l \approx 0.98m_0$ where m_0 is the bare electron mass) and a small mass for perpendicular momentum (transverse mass $m_t \approx 0.19m_0$).

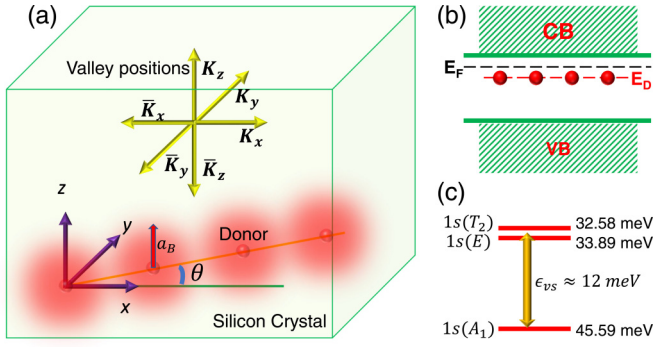

FIG. 1. (a) One-dimensional donor array in a silicon crystal. $K_x/\bar{K}_x$, $K_y/\bar{K}_y$, and $K_z/\bar{K}_z$ label the six Si conduction band valleys centered at $\mathbf{K}_\mu = \pm k_0\hat{x}, \pm k_0\hat{y}, \pm k_0\hat{z}$, where $k_0 = 0.85\pi/a$ and a is the lattice constant of silicon. (b) Donor level E_D and (c) splitting between A_1, E, and T_2 donor states.

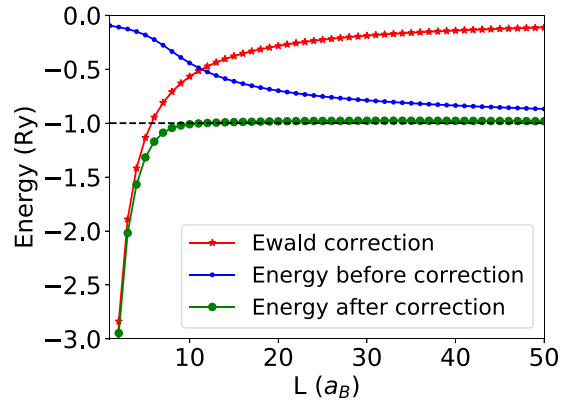

FIG. 2. Bottom of a cubic donor array impurity band vs lattice constant L, neglecting (blue curve) and including (green curve) the Ewald correction (red curve). In the large-L limit, the band narrows exponentially, and when the Ewald correction, required to set the zero of energy correctly in the plane-wave expansion method we employ, is included, it is centered on the energy of an isolated donor. In silicon the Rydberg energy of a donor is Ry $\approx$ 32.6 meV and the effective Bohr radius $a_B \approx 1.9$ nm.

Because we are interested in a periodic array of donors, we use a plane-wave expansion approach and place donors at the center of three-dimensional supercells with dimension $L_x \times L_y \times L_z$. The donor array envelope functions then depend on wave vector $\mathbf{k}$ in the array minizone and can be expanded in the form

$$|F_\mu(\mathbf{k})\rangle = \sum_{\mathbf{G}} C_{\mathbf{G}}(\mathbf{k})|\mathbf{k}+\mathbf{G}\rangle, \tag{3}$$

where $\mathbf{k}$ is the wave vector with $k_i \in (-\pi/L_i, \pi/L_i)$ with $i = x, y, z$. The supercell reciprocal lattice vectors $\mathbf{G} = [n_x 2\pi/L_x, n_y 2\pi/L_y, n_z 2\pi/L_z]$, where n_x, n_y, n_z are integers. The plane-wave representation single-particle Hamiltonian matrix is a sum of kinetic and potential energy contributions:

$$H^{\mathbf{GG}'}_{\mu\mu'}(\mathbf{k}) = T^{\mathbf{GG}'}_{\mu\mu'}(\mathbf{k}) + V^{\mathbf{GG}'}_{\mu\mu'}(\mathbf{k}). \tag{4}$$

The kinetic energy is dependent on the spatial orientation of the donor array relative to the cubic axes. We limit our attention to donor arrays that have their $\hat{z}$ axis aligned with the silicon $\hat{z}$ direction, but allow for changes of orientation θ of the donor array $\hat{x}$ and $\hat{y}$ directions relative to the silicon crystal $\hat{x}$ and $\hat{y}$ axes. For this family of donor array orientations

$$T^{\mathbf{GG}'}_{\mu\mu'} = \delta^{\mathbf{GG}'}_{\mu\mu'} \sum_i \frac{\hbar^2}{2m_i^*}\left[\sum_j (k_j + G_j)R_{ij}(\theta)\right]^2, \tag{5}$$

where $\delta^{\mathbf{GG}'}_{\mu\mu'} \equiv \delta_{\mu\mu'}\,\delta_{\mathbf{GG}'}$ and $R_{ij}(\theta)$ is the rotation matrix. The external potential of the donor array[43] is that produced by unit positive charges at the center of each supercell so that

$$V^{\mathbf{GG}'}_{\mu,\mu'}(\mathbf{k}) = -\frac{1}{\Omega}\delta_{\mu\mu'}\frac{4\pi e^2}{\epsilon|\mathbf{G}-\mathbf{G}'|^2}, \tag{6}$$

where Ω is the supercell volume and $\epsilon \approx 11.7$ is the static dielectric constant of silicon. In silicon, the effective Bohr radius is $a_B = a_0\epsilon/m^* \approx 1.9$ nm and Ry ≈ 32.6 meV. The effective mass approximation is justified by the large value of a_B compared to a lattice constant and the small value of Ry compared to the semiconductor gap. The approximate binding energy is consistent with the experimental value [32,44,45].

As we show explicitly in Fig. 2, when all dimensions of the supercell approach infinity, the envelope functions approach hydrogenic wave functions and the donor binding energies approach Ry $= R_H m^*/\epsilon^2$, where $R_H \approx 13.6$ eV is the electron binding energy of hydrogen in vacuum, and $m^* \equiv (m_t^2 m_l)^{1/3}$ is the conduction band effective mass, which is $\approx 0.33m_0$ with $m_l \approx 0.98m_0$ and $m_t \approx 0.19m_0$.

The one-dimensional donor array case is modeled by choosing large values for two of the supercell lattice constants. The donor states then form one-dimensional bands, and have band dispersion that is strongly valley dependent as illustrated in Fig. 3, and sensitive to the spatial orientation of the donor array relative to the cubic axes. Band dispersion in a valley is weakened in directions close to the longitudinal direction for that valley because of the large longitudinal masses. The hopping parameters in Fig. 3 are extracted from near-neighbor

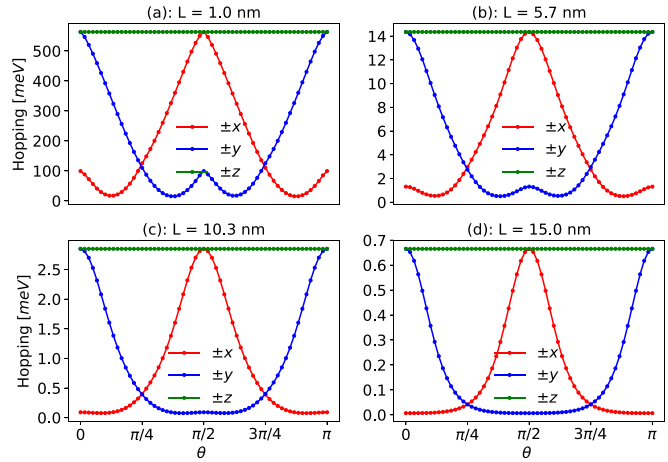

FIG. 3. Valley and orientation dependent near-neighbor hopping parameters for cubic donor arrays with lattice constants L. The $\pm x$, $\pm y$, and $\pm z$ labels specify the Si conduction band valleys centered at $\mathbf{K}_\mu = \pm k_0\hat{x}, \pm k_0\hat{y}, \pm k_0\hat{z}$, where $k_0 = 0.85\pi/a$ and a is the lattice constant of silicon.

tight-binding-model fits to the donor array bands. For the sake of definiteness, we consider donor arrays that are oriented along a direction in the $\hat{x}$-$\hat{y}$ plane specified by orientation angle θ. Hopping within the $\pm z$ valleys is insensitive to the rotation angle θ because its effective mass tensor is invariant under rotations about $\hat{z}$. For the $\pm x$ or $\pm y$ valleys, on the other hand, hopping on the array depends strongly on the the orientation angle. For a $\langle 110\rangle$ orientation the x-valley and y-valley hopping processes have identical amplitudes that are one order of magnitude smaller than for z-valley hopping. Note that hopping is diagonal in valleys, whereas the central cell corrections considered in the following section mix valleys. The interplay between valley mixing at donor cites and valley-dependent tunneling between valleys is responsible for the sensitivity of donor pair and donor array properties to donor placement that we focus on in this paper.

III. CENTRAL CELL CORRECTIONS

So far we have neglected the central cell corrections that are important in silicon and yield donor bound states that couple different valleys. The binding energies observed experimentally are 45.59 meV for the singly degenerate $1s$ (A_1) level [32,44,45], 32.58 meV for the doubly degenerate $1s$ (E) level, and 33.89 meV for the triply degenerate $1s$ (T_2) level. If we ignore the small difference between the $1s$ (E) and $1s$ (T_2) levels, we can approximate the central cell correction correction to the single-particle Hamiltonian as the product of a single valley splitting energy scale $\epsilon_{vs} \approx 12$ meV [32,46], an attractive delta function $-\epsilon_{vs}\delta(\mathbf{r}-\mathbf{R})$ at the donor site $\mathbf{R}$, and a projection onto the donor states,

$$\mathcal{H}_{vs}(\mathbf{R}) = \frac{-\epsilon_{vs}}{N_\mu \Omega} \sum_{\substack{\mathbf{k}'\mathbf{k} \\ \mu'\mu}} |\mathbf{k}'\mu'\rangle\langle\mathbf{k}\mu|\, e^{i(\mathbf{K}_\mu+\mathbf{k}-\mathbf{K}_{\mu'}-\mathbf{k}')\cdot\mathbf{R}}, \tag{7}$$

where $\mathbf{K}_\mu = \pm k_0\hat{x}, \pm k_0\hat{y}, \pm k_0\hat{z}$ are valley momenta in bulk silicon, $k_0 = 0.85(2\pi/a)$, and $a = 0.543$ nm is the conventional cubic lattice constant of bulk silicon. Because $\mathbf{K}_\mu - \mathbf{K}_{\mu'}$ is comparable in size to a reciprocal lattice vector, the valley splitting Hamiltonian changes substantially even for changes in $\mathbf{R}$ that are on the atomic length scale. Note that Eq. (7) contains $\mu' \neq \mu$ terms that couple different valleys.

In order to calculate the parameters of a generalized Hubbard model for the donor array, we first Fourier-transform the wave functions in the lowest energy band back to real space:

$$|\mathbf{R}\mu\sigma\rangle = \sum_{\mathbf{k},\mathbf{G}} C^{\mu\sigma}_{\mathbf{kG}} e^{-i\mathbf{k}\cdot\mathbf{R}} |\mathbf{k}+\mathbf{K}_\mu+\mathbf{G}\rangle|\sigma\rangle, \tag{8}$$

where μ labels valley, σ labels spin, $\mathbf{R}$ is the position of the donor, and we have chosen $C_{\mathbf{kG}=0}$ to be real and positive at each value of $\mathbf{k}$. The single-particle Hamiltonian in the Wannier representation defines the donor array hopping parameters $t^{\mu\mu'}_{\mathbf{RR}'}$, which are a sum of kinetic energy ($T_{\mathbf{RR}'}$) and external potential ($V^{\text{ext}}_{\mathbf{RR}'}$) contributions, with details shown in Appendix B.

In Figs. 4(a) and 4(b) we plot hopping parameters for the $\pm x$ and $\pm y$ valleys as a function of donor separation and the spatial orientation of the donor array relative to the x axis. We see here that at small donor distances minima of the hopping parameters appear at $\theta \approx \pi/8$ for $\pm x$ valleys and at $\theta \approx 3\pi/8$ for $\pm y$ valleys, while for the $\pm z$ valley, the hopping parameters are independent of θ and the decay lengths of the hopping parameters extracted from the valley wave functions are nearly independent of θ. In the $\langle 100\rangle$ direction both $\pm y$ and $\pm z$ effective masses are transverse (m_t) and therefore have the same decay length, which is larger than the $\pm x$ valley decay length which has the longitudinal effective mass m_l. Similar results apply for the $\pm x$ and $\pm z$ valleys in the 010 direction. Along the $\langle 110\rangle$ direction ($\theta = \pi/4$) the decay lengths of the $\pm x$ and $\pm y$ valleys are identical since the wave functions have equal contributions from transverse and longitudinal mass components.

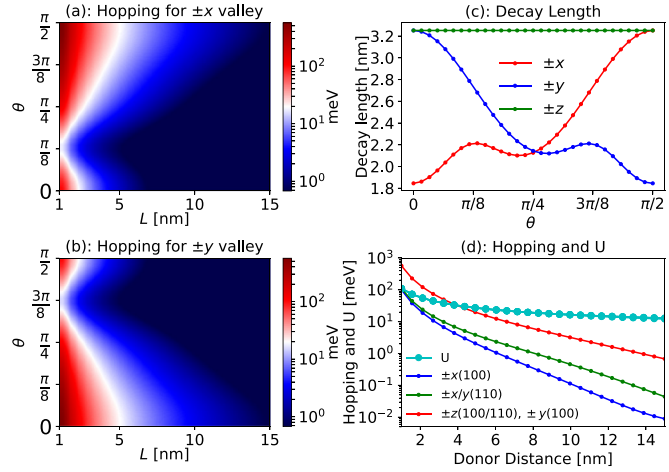

FIG. 4. Hopping parameters and on-site interactions of the silicon donor array Hubbard model vs donor separation and spatial orientation of the donor array relative to the crystal x axis. The color scale plots in (a) and (b) show the hopping parameter vs donor separation L and spatial orientation θ. (c) Decay lengths vs θ for valley $\pm x$, $\pm y$, and $\pm z$. (d) Hubbard U and hopping parameters for donor arrays along the $\langle 100\rangle$ and $\langle 110\rangle$ directions.

The on-site Hubbard U can be calculated using $U_{\mu\mu'} = \langle \mathbf{R}\mu\sigma, \mathbf{R}\mu'\sigma|V_c|\mathbf{R}\mu\sigma, \mathbf{R}\mu'\sigma\rangle$ where $|\mathbf{R}\mu\sigma\rangle$ is a Wannier function and $V_c = e^2/\epsilon r^2$. In Fig. 4(d) we compare hopping parameters for donor arrays along the $\langle 100\rangle$ and $\langle 110\rangle$ directions At small donor separation, valleys with transverse mass have larger hopping parameters that are large compared with U. However on-site electron-electron interaction strengths exceed the hopping parameters at larger donor separations; the ratio reaches $\sim$10 when the donor separation is around 12 nm.

IV. VALLEY INTERFERENCE AND EXCHANGE INTERACTIONS

Using the Hubbard model parameters discussed above, we now assess the influence of valley degeneracy and donor placement on the exchange interactions between neighboring sites of a donor array. To calculate the exchange interactions we study a two-site Hubbard model which includes hopping, valley splitting, and on-site electron-electron interaction

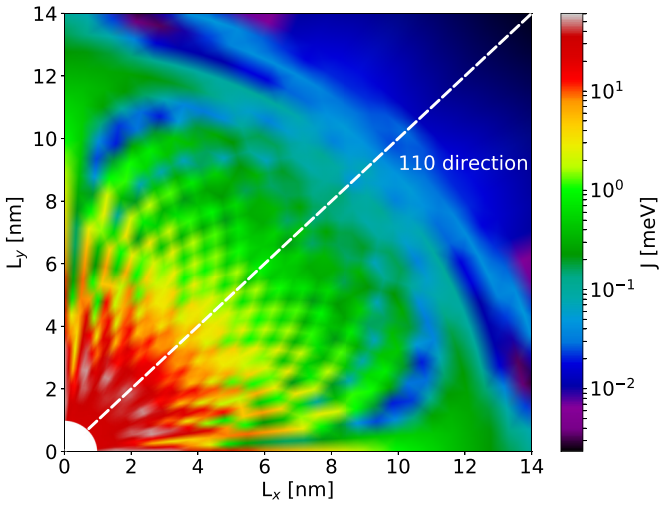

FIG. 5. Exchange interaction between two donors calculated with a two-site six-orbital Hubbard model. In explicit calculations, we place one of the two donors at the origin and the other at $\mathbf{L} = L(1, 0, 0)$, where L is the distance between two donors, and rotate the host-crystal cubic lattice by angle θ. The mapping from an L-θ grid to the plotted L_x-L_y grid leads to some (white) regions in which there are no data. The white line labels the $\langle 110 \rangle$ direction.

terms:

$$H = \sum_{\nu} t_{\mu}(c^{\dagger}_{1\mu\sigma}c_{2\mu\sigma} + \text{H.c.}) + \epsilon_{vs}\sum_{i,\mu\mu'} P^{i}_{\mu\mu'}c^{\dagger}_{i\mu\sigma}c_{i\mu'\sigma} + \sum_{i\mu\mu'\sigma\sigma'} U_{\mu\mu'}c^{\dagger}_{i\mu\sigma}c_{i\mu\sigma}c^{\dagger}_{i\mu'\sigma'}c_{i\mu'\sigma'}. \quad (9)$$

Here t_{μ} is the intersite hopping amplitude within valley $\mathbf{K}_{\mu}$, $c^{\dagger}_{i\mu\sigma}$ ($c_{i\mu\sigma}$) is a creation (annihilation) operator, $P^{i}_{\mu\mu'} = e^{i(\mathbf{K}_{\mu}-\mathbf{K}_{\mu'})\cdot\mathbf{R}}$ is the operator that applies a central cell energy shift at site $\mathbf{R}$ to the donor state, and $U_{\mu\mu'}$ is the on-site electron-electron interaction, which can be accurately modeled as valley independent. For one electron per donor, the charge excitation sector is gaped and low-energy states are formed from spin degrees on each site. The exchange interaction between spins can therefore be defined in terms of the energy difference between the lowest-energy two-electron singlet and triplet states: $J = E_T - E_S$.

In Fig. 5 we plot the exchange interaction vs donor separation magnitude and direction. In our explicit calculations we place one of the two donors at the origin and the other at $\mathbf{L} = L(1, 0, 0)$, where L the distance between two donors, and rotate the host-crystal cubic lattice by angle θ. The $\pm z$ valleys always have a transverse effective mass m_t, which leads to large intersite hopping amplitudes. Because the displacement $\mathbf{L}$ is perpendicular to the $\pm z$ valley momenta $\mathbf{K}_{\mu}$, the phase factors in the $(\pm z, \pm z)$ blocks of the valley-splitting Hamiltonian always vanish (i.e., $\hat{z}\cdot\mathbf{L} = 0$, with $\mathbf{L} \equiv \mathbf{R} - \mathbf{R}'$). For general θ both the $\pm x$ and $\pm y$ blocks of the valley splitting Hamiltonian at $\mathbf{L}$ have nontrivial phase factors, which change in value when L changes on an atomic length scale, and appear in the hopping amplitude between the two A_1 exciton levels. For $\theta = 0$ ($\theta = \pi/2$), $\pm x$ ($\pm y$) valley hopping is longitudinal, and is therefore dominated by $\pm y$ ($\pm x$) and $\pm z$ valley components. It follows that the exchange energy is not sensitive to atomic scale position variations along the direction of the array, since both $\hat{y}\cdot\mathbf{L}$ ($\hat{x}\cdot\mathbf{L}$) and $\hat{z}\cdot\mathbf{L}$ are 0. However, there is a strong sensitivity to donor position variations in the direction perpendicular to donor array. In the $\langle 110 \rangle$ direction, the sensitivity of exchange interactions to donor placement is reduced in all in-plane directions since both $\pm x$ and $\pm y$ valley hopping strengths are reduced relative to $\pm z$ valley hopping. These results are consistent with recent experiments which have demonstrated a valley filtering effect on exchange interactions [35,36], which is captured with a very simple model in this paper. As we explain in more detail in the next section, the lowest-energy states become more concentrated in A_1 valley-split states at large donor separation, where ϵ_{vs} is larger than the hopping energies. The problem of exchange splitting has been considered previously [47] using the approximation, valid at large L, that the impurity state Hamiltonian can be projected onto the A_1 basis, with qualitatively similar results for the large-L limit.

V. DISORDERED ONE-DIMENSIONAL ELECTRONS

Donor placement in silicon often errs by a lattice constant or more. Even when a regular one-dimensional donor array is intended, the actual positions are $R_i = (n_i N_i + \delta_i)a\hat{r}_i$, where $\delta_i = 0, \pm 1$ randomly. Here $i = x, y, z$ and $\hat{r}_i = \hat{x}, \hat{y}, \hat{z}$ are unit vectors along cubic axes, and N_i is the intended superlattice length in units of the silicon lattice constant a. As we see from Eq. (7), the random displacements introduce random phase factors $\exp i(\mathbf{K}_{\mu} - \mathbf{K}_{\mu'})\cdot\mathbf{R}$ in the off-diagonal matrix elements of the valley-splitting Hamiltonian (see the appendices for further details). These phase factors account for changes in the positions at which the system gains energy by establishing constructive interference between valleys. The phase factors are sensitive to atomic scale placement inaccuracy because valley momenta are comparable in size to microscopic silicon primitive reciprocal lattice vectors, and much larger than the donor array superlattice primitive reciprocal lattice vectors. To study the influence of donor positional disorder on electronic properties we neglect interactions and calculate localization lengths using transfer matrices [48] for a model in which the $\exp(i\mathbf{K}_{\mu}\cdot\mathbf{R})$ ($\mu = x, y$) factors are modeled as independent random phase factors with phases Φ_{μ}. $\Phi_z = 0$ because the vertical component of the donor position is not expected to be disordered.

The Bloch state spectrum of donor arrays placed in the $\langle 100 \rangle$ and $\langle 110 \rangle$ directions are shown in Fig. 6(a). In the $L = 12$ nm case, illustrated in Fig. 6(b), we see that the A_1 subband (lowered by ϵ_{vs}) is split out, and that the width of this subband corresponds to an effective hopping amplitude that is intermediate between the longitudinal and $\hat{z}$-direction values, which will be discussed further below.

The donor array orientation dependence of our results is most easily understood in the large-ϵ_{vs} limit, where we can truncate the Hilbert space to the A_1 donor levels. The amplitude for hopping between A_1 levels is

$$t_{A1} = \frac{1}{6}\sum_{\mu} t_{\mu}\exp(i\Phi_{\mu}) \quad (10)$$

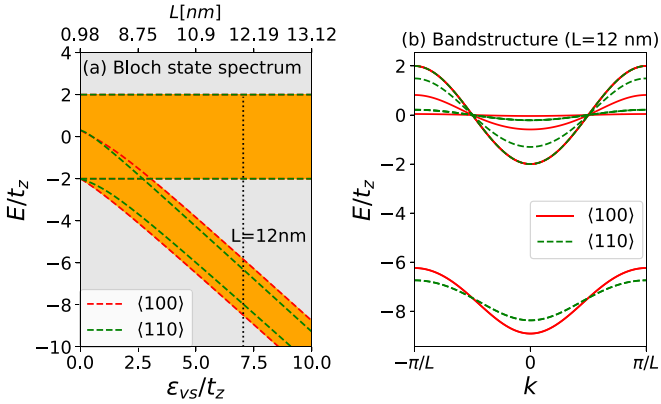

FIG. 6. (a) Bloch state spectrum vs valley splitting strength $\epsilon_{vs} =$ 12 meV. Energies are in units of the hopping energy t_z. The corresponding donor separation L is indicated along the upper horizontal axis. The green and red dashed lines specify the band edges for donors placed along the ⟨110⟩ and ⟨100⟩ directions, respectively, and the orange regions are inside at least one of the six donor array bands for one of the two orientations. (b) Quasi-1D band structures for $L = 12$ nm donor arrays along the ⟨100⟩ and ⟨110⟩ directions, respectively. The lowest energy (valley-split) A_1 band is singly degenerate in both cases. In the ⟨100⟩ (⟨100⟩) case the top dispersive (middle flatter) band with width of $4t_z$ ($4t_{x/y}$) has degeneracy of 3.

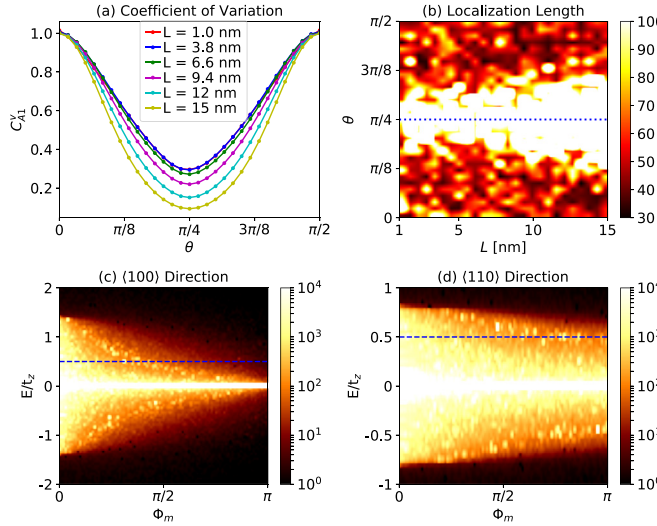

FIG. 7. (a) Coefficient of variation for hopping between A_1 states. Note that disorder is increasingly minimized at $\theta = \pi/4$ as L increases. (b) Localization in donor separation units vs donor separation L and the orientation of the donor array relative to the x axis θ at an energy $E = 0.5t_z$ above the middle of the disordered A_1 band. (c) and (d) illustrate the dependence of A_1 band localization length on disorder strength and energy for $L = 12$ nm. The dashed lines in (c) and (d) mark $E = 0.5t_z$, the energy used in (b).

with $\Phi_z = 0$ and Φ_x and Φ_y imposed by random $\hat{x}$-$\hat{y}$ plane positional shifts of the two donors. Averaging over these phases we find that $\langle t_{A1}\rangle = t_z/3$ and the coefficient of variation (the square root of the variance divided by the mean) is

$$C^v_{A1} = \frac{\sigma_{A1}}{\langle t_{A1}\rangle} = \frac{\sqrt{t_x^2 + t_y^2}}{t_z}. \tag{11}$$

Here σ^2_{A1} is the variance of t_{A1} and $\langle t_{A1}\rangle$ is its average value. The coefficient of variation for t_{A1} is dominated by the larger of t_x and t_y, and therefore reaches a minimum when $\theta = \pi/4$ since both t_x and t_y are reduced compared to t_z in this case. In Fig. 7(a) we plot C^v_{A1} vs θ for a series of L values. Here we see that the coefficient of variation of the hopping amplitude is close to 1 at $\theta = 0$, but reaches a minimum that drops with donor separation L at $\theta = \pi/4$. Hopping disorder is weaker for donor arrays aligned along ⟨110⟩ directions.

As a result of this reduced disorder, the localization lengths of the A_1 band electrons reach a maximum at $\theta = \pi/4$. The localization lengths are defined as the inverse of the smallest positive Lyapunov exponent averaged over phase disorder realizations: $\xi_{\rm loc} = \langle\gamma_m\rangle^{-1}_{\rm avg}$ (see the appendices for further details). In Fig. 7(b) we plot localization lengths calculated at an energy $0.5t_z$ from the center of the disordered A_1 band, with $\Phi_{x/y}$ sampled from the interval $(-\Phi_m, \Phi_m)$ and $\Phi_m = \pi/2$; we see that the localization lengths maximize at ⟨110⟩ direction. The A_1 band localization lengths are plotted vs energy and Φ_m for $L = 12$ nm in Figs. 7(c) and 7(d) for the ⟨100⟩ and ⟨110⟩ directions, respectively. For ⟨110⟩-orientation donor arrays, localization lengths remain long near the center of the A_1 band, even for strong donor-placement disorder.

VI. DISCUSSION

In this paper, we have considered the valley physics of donor pairs and donor arrays in bulk silicon in which the valleys are sixfold degenerate. As we have explained in detail, the combination of central cell interactions that couple valleys and valley-dependent tunneling amplitudes between donor sites yields valley interference effects responsible for undesirable sensitivity to atomic length scale errors in donor placement. The complications introduced by the valley degree of freedom in silicon donor qubit design can be, and are in practice, mitigated in a variety of ways. In fact lattice-matching strain effects and positioning of donors very close to the surface fully lifts the valley degeneracy. Even so, these valley splittings are often not large, allowing valleys to play a role in setting the size and orientation dependence of exchange interactions which remain sensitive to atomic scale placement uncertainty. The approach taken in this paper provides a practical but accurate theoretical model that applies equally well when valley degeneracy is lifted, and may be valuable in achieving a quantitative understanding of the properties of donor systems used for quantum information processing.

Our model is based on the observations that there is an increase in donor binding energy ϵ_{vs} when all valley components of the donor wave function are in phase at the donor site. For donor separations less than ∼4 nm, all six silicon valleys play an important role in low-energy many-electron states. At larger L, valley-splitting exceeds hopping energies and the low-energy physics can be approximated by an A_1 one-band model. Because the valley wave vectors are well separated in silicon, valley splitting leads to strong disorder in the hopping amplitude between the most strongly bound donor states, even when inaccuracy in donor placement is only

at the microscopic silicon lattice constant scale. It follows from our model that silicon donor arrays provide an excellent quantum simulator to study the combined influence of strong interactions and strong disorder in one dimension.

The importance of interactions in silicon donor array states can be judged by evaluating the on-site Hubbard U. $U \sim 10$ meV exceeds the hopping parameters at larger donor separations, reaching a ratio of ~ 10 when the donor separation is around 12 nm. In this limit only spin degrees of freedom are relevant. Donor arrays are thus an attractive platform of quantum simulator to study the physics in one or two dimensional disordered many-body models, such as random field Heisenberg models [49] and one-dimensional Hubbard physics with hopping disorder [50–52]. In the limit of large L disorder can be weakened, but not eliminated, by orienting the donor array along the $\langle 110 \rangle$ direction.

ACKNOWLEDGMENTS

This work was supported by the U.S. Department of Energy, Office of Science, Basic Energy Sciences, under Award # DE-SC0022106. We acknowledge the generous HPC resources provided by Texas Advanced Computing Center (TACC) at the University of Texas at Austin.

APPENDIX A: EWALD CORRECTIONS

Subtleties arise in using a momentum space approach to obtain energy spectrum of electrons attracted to a donor array because the long-range of the Coulomb interaction forces used to exclude the $\mathbf{G} = 0$ term in the external potential. Corrections in momentum space and real space can be combined into an Ewald correction [43]

$$\delta E = \sum_{\mathbf{R}\neq 0} \frac{e^2}{R} e^{-\kappa R} - \int \frac{ne^2}{r} \cdot d\mathbf{r}, \tag{A1}$$

where $R = |\mathbf{R}|$ with $\mathbf{R} = [n_x L_x, n_y L_y, n_z L_z]$, $r = |\mathbf{r}|$, $n = \frac{1}{\Omega}$, $\Omega = L_x \times L_y \times L_z$ is the volume of the supercell, and κ is a convergence parameter that can be set to zero at the end of the calculation. The first term in Eq. (A1) is summed over nonzero array lattice vectors. The factor $e^{-\kappa R}$ is introduced to regularize the Coulomb interaction, which is recovered by letting $\kappa \to 0$. By employing the identity

$$\frac{1}{R} = \left(\frac{\eta}{\pi}\right)^{\frac{1}{2}} \int_0^\infty dt\, t^{-\frac{1}{2}} e^{-\eta t R^2}, \tag{A2}$$

which holds for any positive value of η, the first term in Eq. (A1) can finally be written as

$$\delta E = -6n^{\frac{1}{3}} + \sum_{\mathbf{R}\neq 0} \phi_{-\frac{1}{2}(\pi n^{\frac{2}{3}} R^2)} + \sum_{\mathbf{G}\neq 0} \phi_0\left(\frac{G^2}{4\pi n^{\frac{2}{3}}}\right) + \int d\mathbf{R} \frac{ne^2}{R}, \tag{A3}$$

where $\phi_\mu(z) \equiv \int_1^\infty dt\, e^{-zt} t^\mu$ is the Misra function. Note that the last term in Eq. (A3) is divergent, but cancels the second term in Eq. (A1) [43]. The Ewald correction to the donor band levels is then

$$\delta E = -6n^{\frac{1}{3}} + \sum_{\mathbf{R}\neq 0} \phi_{-\frac{1}{2}(\pi n^{\frac{2}{3}} R^2)} + \sum_{\mathbf{G}\neq 0} \phi_0\left(\frac{G^2}{4\pi n^{\frac{2}{3}}}\right). \tag{A4}$$

The Ewald correction has a $1/L$ dependence [43] as shown in Fig. 2. When the Ewald correction is $k = 0$ the donor band state is close to the hydrogenic binding energies for supercell dimensions that exceed around $10a_B$. For the small donor separations, the donor bands disperse and the $k = 0$ state is at the bottom of the donor array band.

APPENDIX B: WANNIER BASIS

Without considering the valley splitting, the Wannier functions are defined as

$$|\mathbf{R}\rangle = \frac{1}{\sqrt{N_\mathbf{k}}} \sum_{\mathbf{k},\mathbf{G}} C^{(1)}_{\mathbf{k},\mathbf{G}} e^{-i\mathbf{k}\cdot\mathbf{R}} |\mathbf{k}+\mathbf{G}\rangle. \tag{B1}$$

Here we can choose $C^{(1)}_{\mathbf{k},\mathbf{G}}$ to be real and positive for $\mathbf{G} = \mathbf{0}$ and the superscript (1) denotes the ground state. $\mathbf{R}$ is the lattice vectors of supercell. The basis projected onto the real space is then

$$\langle \mathbf{r}|\mathbf{R}\rangle = \sum_{\mathbf{k},\mathbf{G}} C^{(1)}_{\mathbf{k},\mathbf{G}} e^{-i\mathbf{k}\cdot\mathbf{R}} \langle \mathbf{r}|\mathbf{k}+\mathbf{G}\rangle. \tag{B2}$$

It is easy to show that the Wannier functions are orthogonal, i.e., $\langle \mathbf{R}'|\mathbf{R}\rangle = \delta_{\mathbf{R}'\mathbf{R}}$. Here we used the fact that

$$\langle \mathbf{k}'+\mathbf{G}'|\mathbf{k}+\mathbf{G}\rangle = \delta_{\mathbf{k}'\mathbf{k}} \delta_{\mathbf{G}'\mathbf{G}}. \tag{B3}$$

When we include valley and spin freedom, the Wannier function becomes

$$|\mathbf{R}\mu\sigma\rangle = \sum_{\mathbf{k},\mathbf{G}} C^{\mu\sigma}_{\mathbf{k},\mathbf{G}} e^{-i\mathbf{k}\cdot\mathbf{R}} |\mathbf{k}+\mathbf{k}_\mu+\mathbf{G}\rangle|\sigma\rangle. \tag{B4}$$

The single-particle Hamiltonian in the Wannier representation defines the donor array hopping parameters $t^{\mu\mu'}_{\mathbf{R}\mathbf{R}'}$, which are contributed by the kinetic energy ($T_{\mathbf{R}\mathbf{R}'}$) and external potential ($V^{\text{ext}}_{\mathbf{R}\mathbf{R}'}$). The kinetic term contribution is

$$T^{\mathbf{R}\mathbf{R}'}_{\mu\mu'} = \frac{\delta_{\mu\mu'}}{N_k} \sum_{i\mathbf{k}\mathbf{G}} |C_{\mathbf{k}\mathbf{G}}|^2 \frac{\hbar^2}{2m_i} (k_i + G_i)^2 e^{i\mathbf{k}\cdot(\mathbf{R}-\mathbf{R}')}, \tag{B5}$$

where $i = x, y, z$, $N_\mathbf{k}$ is the total number of sampling points in the Brillouin zone, and $C_{\mathbf{k}\mathbf{G}}$ is the momentum space Bloch state eigenvector. And the external potential contribution is

$$V^{\mathbf{R}\mathbf{R}'}_{\text{ext}} = \frac{1}{N_k} \sum_{\mathbf{k}\mathbf{G}\mathbf{G}'} C^*_{\mathbf{k}\mathbf{G}'} C_{\mathbf{k}\mathbf{G}} e^{i\mathbf{k}\cdot(\mathbf{R}'-\mathbf{R})} V(\mathbf{G}'-\mathbf{G}), \tag{B6}$$

where $V(\mathbf{G}'-\mathbf{G}) = 2\pi e^2/\epsilon|\mathbf{G}'-\mathbf{G}|$ is the external potential from the donors. Note that the Wannier representation single-particle Hamiltonian is independent of the gauge choice made in defining the Wannier functions.

APPENDIX C: CENTRAL CELL CORRECTION

The central cell correction Hamiltonian is approximated as

$$\mathcal{H}_{vs} = -\sum_{\mathbf{R}} \epsilon_{vs} \delta(\mathbf{r}-\mathbf{R}); \tag{C1}$$

here $\mathbf{R}$ is the lattice vector of impurities supercell and ϵ_{vs} is the valley splitting. The matrix elements in momentum space are then

$$\mathcal{H}_{vs}(\mathbf{k}) = \langle \mathbf{k} + \mathbf{K}'_\mu + \mathbf{G}'|H_{cc}|\mathbf{k} + \mathbf{K}_\mu + \mathbf{G}\rangle \delta_{\sigma\sigma'} = -\frac{\epsilon_{vs}}{N_\mu \Omega} \sum_{\mathbf{R}} e^{i(\mathbf{K}_\mu - \mathbf{K}_{\mu'})\cdot\mathbf{R}} \delta_{\sigma\sigma'}. \quad \text{(C2)}$$

Here $N_\mu = 6$ is the number of valleys. The calculations of $\sum_{\mathbf{L}} e^{i(\mathbf{K}_\mu - \mathbf{K}_{\mu'})\cdot\mathbf{R}}$ strongly depend on the inaccuracies of positions of donors. In silicon the position of the valley is $\mathbf{K}_\mu = \pm k_0\hat{x}, \pm k_0\hat{y}, \pm k_0\hat{z}$. For perfect periodic impurities, the matrix elements coupling different valleys should be $-\frac{\epsilon_{vs}}{N_\mu\Omega}$; the matrix is then

$$\mathcal{H}_{vs}(\mathbf{k}) = -\frac{\epsilon_{vs}}{6\Omega}\begin{bmatrix} 1 & 1 & 1 & 1 & 1 & 1 \\ 1 & 1 & 1 & 1 & 1 & 1 \\ 1 & 1 & 1 & 1 & 1 & 1 \\ 1 & 1 & 1 & 1 & 1 & 1 \\ 1 & 1 & 1 & 1 & 1 & 1 \\ 1 & 1 & 1 & 1 & 1 & 1 \end{bmatrix}. \quad \text{(C3)}$$

When the periodicity of impurities is not perfect, the diagonal matrix elements are still all 1. However, the off-diagonal matrix elements are $e^{i\Phi}$, in which Φ is a random phase; the matrix is

$$\mathcal{H}_{vs}(\mathbf{k}) = -\frac{\epsilon_{vs}}{6\Omega}\begin{bmatrix} 1 & e^{i2\Phi_x} & e^{i(\Phi_x-\Phi_y)} & e^{i(\Phi_x+\Phi_y)} & e^{i(\Phi_x-\Phi_z)} & e^{i(\Phi_x+\Phi_z)} \\ e^{-i2\Phi_x} & 1 & e^{i(-\Phi_x-\Phi_y)} & e^{i(-\Phi_x+\Phi_y)} & e^{i(-\Phi_x-\Phi_z)} & e^{i(-\Phi_x+\Phi_z)} \\ e^{i(\Phi_y-\Phi_x)} & e^{i(\Phi_y+\Phi_x)} & 1 & e^{i2\Phi_y} & e^{i(\Phi_y-\Phi_z)} & e^{i(\Phi_y+\Phi_z)} \\ e^{i(-\Phi_y-\Phi_x)} & e^{i(-\Phi_y+\Phi_x)} & e^{-i2\Phi_y} & 1 & e^{i(-\Phi_y-\Phi_z)} & e^{i(-\Phi_y+\Phi_z)} \\ e^{i(\Phi_z-\Phi_x)} & e^{i(\Phi_z+\Phi_x)} & e^{i(\Phi_z-\Phi_y)} & e^{i(\Phi_z+\Phi_y)} & 1 & e^{i2\Phi_z} \\ e^{i(-\Phi_z-\Phi_x)} & e^{i(-\Phi_z+\Phi_x)} & e^{i(-\Phi_z-\Phi_y)} & e^{i(-\Phi_z+\Phi_y)} & e^{-i2\Phi_z} & 1 \end{bmatrix}. \quad \text{(C4)}$$

APPENDIX D: LOCALIZATION LENGTH

With the Wannier basis, the general form of the Hamiltonian is

$$H = \sum_{i\mu, j\mu'} t_{i\mu, j\mu'} |i\mu\rangle\langle j\mu'| + \frac{\epsilon_{vs}}{6} \sum_{i\mu\mu'} P^i_{\mu\mu'} |i\mu\rangle\langle i\mu'|, \quad \text{(D1)}$$

where $|i\mu\rangle$ labels the states that lie at the ith site and μ is the valley freedom, $t_{i\mu,j\mu'}$ are the hopping parameters, ϵ_{vs} is the valley splitting, and $P^i_{\mu\mu'}$ is the projector operator as $e^{i(\mathbf{K}_\mu - \mathbf{K}_{\mu'})\cdot\mathbf{R}}$, which is modeled as three random phases shown in Eq. (C4). The localization length is calculated with a transfer matrix method; the Schrödinger equation can be rewritten as

$$-\mathbb{t}_{i-1,i}\chi_{i-1} + \mathbb{v}_i\chi_i - \mathbb{t}_{i,i+1}\chi_{i+1} = E\chi_i, \quad \text{(D2)}$$

where $\mathbb{t}_{ij}$ is the hopping matrix between the sites i and j, $\mathbb{v}_i$ is the valley matrix at site i, and χ_i are the wave function components, while the wave function of the Hamiltonian is $\Psi = [\chi_1\chi_2\cdots\chi_i\cdots\chi_N]^T$. The $2N_\mu \times 2N_\mu$ transfer matrix is

$$\mathbb{M}_i = \begin{bmatrix} \mathbb{t}^{-1}_{i,i+1}(\mathbb{v}_i - E\mathbb{1}) & -\mathbb{t}^{-1}_{i,i+1}\mathbb{t}_{i-1,i} \\ \mathbb{1} & \mathbb{0} \end{bmatrix}. \quad \text{(D3)}$$

When considering only the A_1 state, the transfer matrix is

$$\mathbb{M}_i = \begin{bmatrix} E/t_{A1} & -1 \\ 1 & 0 \end{bmatrix}, \quad \text{(D4)}$$

with $t_{A1} = \frac{1}{6}\sum_\mu t_\mu \exp(i\Phi_\mu)$. The transfer matrix product for the whole system of length N is

$$\mathbb{M} = \prod_{i=1}^{N} \mathbb{M}_i, \quad \text{(D5)}$$

and then we can write

$$\begin{bmatrix} \chi_{N+1} \\ \chi_N \end{bmatrix} = \mathbb{M}\begin{bmatrix} \chi_1 \\ \chi_0 \end{bmatrix}. \quad \text{(D6)}$$

According to Oseledec's theorem [53], the eigenvalues λ_j of the matrix

$$\Omega = \ln(\mathbb{M}_N\mathbb{M}_N^\dagger) \quad \text{(D7)}$$

obey the following:

$$\gamma_j = \lim_{N\to\infty} \frac{\lambda_j}{2N}, \quad \text{(D8)}$$

which are called Lyapunov exponents. The smallest positive Lyapunov exponent averaged over a random configuration is the inverse of localization length:

$$\langle\gamma_m\rangle_{\text{avg}} = \frac{1}{\xi_{\text{loc}}}; \quad \text{(D9)}$$

then we can get the localization length as

$$\xi_{\text{loc}} = \langle\gamma_m\rangle^{-1}_{\text{avg}}, \quad \text{(D10)}$$

where $\langle\ \rangle_{\text{avg}}$ denotes the configuration average of disorder.

[1] F. A. Zwanenburg, A. S. Dzurak, A. Morello, M. Y. Simmons, L. C. L. Hollenberg, G. Klimeck, S. Rogge, S. N. Coppersmith, and M. A. Eriksson, Silicon quantum electronics, Rev. Mod. Phys. **85**, 961 (2013).

[2] P. L. Knight, E. A. Hinds, M. B. Plenio, R. G. Clark, R. Brenner, T. M. Buehler, V. Chan, N. J. Curson, A. S. Dzurak, E. Gauja, H. S. Goan, A. D. Greentree, T. Hallam, A. R. Hamilton, L. C. L. Hollenberg, D. N. Jamieson, J. C. McCallum, G. J. Milburn, J. L. O'Brien, L. Oberbeck *et al.*, Progress in silicon-based quantum computing, Philos. Trans. R. Soc. London, Ser. A **361**, 1451 (2003).

[3] J. J. Pla, K. Y. Tan, J. P. Dehollain, W. H. Lim, J. J. L. Morton, D. N. Jamieson, A. S. Dzurak, and A. Morello, A single-atom electron spin qubit in silicon, Nature (London) **489**, 541 (2012).

[4] H. Büch, S. Mahapatra, R. Rahman, A. Morello, and M. Y. Simmons, Spin readout and addressability of phosphorus-donor clusters in silicon, Nat. Commun. **4**, 2017 (2013).

[5] C. C. Lo, C. D. Weis, J. van Tol, J. Bokor, and T. Schenkel, All-Electrical Nuclear Spin Polarization of Donors in Silicon, Phys. Rev. Lett. **110**, 057601 (2013).

[6] J. J. Pla, F. A. Mohiyaddin, K. Y. Tan, J. P. Dehollain, R. Rahman, G. Klimeck, D. N. Jamieson, A. S. Dzurak, and A. Morello, Coherent Control of a Single ^{29}Si Nuclear Spin Qubit, Phys. Rev. Lett. **113**, 246801 (2014).

[7] R. Kalra, A. Laucht, C. D. Hill, and A. Morello, Robust Two-Qubit Gates for Donors in Silicon Controlled by Hyperfine Interactions, Phys. Rev. X **4**, 021044 (2014).

[8] A. J. Sigillito, A. M. Tyryshkin, T. Schenkel, A. A. Houck, and S. A. Lyon, All-electric control of donor nuclear spin qubits in silicon, Nat. Nanotechnol. **12**, 958 (2017).

[9] M. Veldhorst, C. H. Yang, J. C. C. Hwang, W. Huang, J. P. Dehollain, J. T. Muhonen, S. Simmons, A. Laucht, F. E. Hudson, K. M. Itoh, A. Morello, and A. S. Dzurak, A two-qubit logic gate in silicon, Nature (London) **526**, 410 (2015).

[10] Y. He, S. Gorman, D. Keith, L. Kranz, J. Keizer, and M. Simmons, A two-qubit gate between phosphorus donor electrons in silicon, Nature (London) **571**, 371 (2019).

[11] K. J. Morse, R. J. S. Abraham, A. DeAbreu, C. Bowness, T. S. Richards, H. Riemann, N. V. Abrosimov, P. Becker, H.-J. Pohl, M. L. W. Thewalt, and S. Simmons, A photonic platform for donor spin qubits in silicon, Sci. Adv. **3**, e1700930 (2017).

[12] S. J. Hile, L. Fricke, M. G. House, E. Peretz, C. Y. Chen, Y. Wang, M. Broome, S. K. Gorman, J. G. Keizer, R. Rahman, and M. Y. Simmons, Addressable electron spin resonance using donors and donor molecules in silicon, Sci. Adv. **4**, eaaq1459 (2018).

[13] J. P. Dehollain, J. T. Muhonen, K. Y. Tan, A. Saraiva, D. N. Jamieson, A. S. Dzurak, and A. Morello, Single-Shot Readout and Relaxation of Singlet and Triplet States in Exchange-Coupled ^{31}P Electron Spins in Silicon, Phys. Rev. Lett. **112**, 236801 (2014).

[14] M. A. Broome, T. F. Watson, D. Keith, S. K. Gorman, M. G. House, J. G. Keizer, S. J. Hile, W. Baker, and M. Y. Simmons, High-Fidelity Single-Shot Singlet-Triplet Readout of Precision-Placed Donors in Silicon, Phys. Rev. Lett. **119**, 046802 (2017).

[15] D. M. Zajac, A. J. Sigillito, M. Russ, F. Borjans, J. M. Taylor, G. Burkard, and J. R. Petta, Resonantly driven CNOT gate for electron spins, Science **359**, 439 (2018).

[16] T. F. Watson, S. G. J. Philips, E. Kawakami, D. R. Ward, P. Scarlino, M. Veldhorst, D. E. Savage, M. G. Lagally, M. Friesen, S. N. Coppersmith *et al.*, A programmable two-qubit quantum processor in silicon, Nature (London) **555**, 633 (2018).

[17] M. A. Broome, S. K. Gorman, M. G. House, S. J. Hile, J. G. Keizer, D. Keith, C. D. Hill, T. F. Watson, W. J. Baker, L. C. L. Hollenberg *et al.*, Two-electron spin correlations in precision placed donors in silicon, Nat. Commun. **9**, 980 (2018).

[18] Y. Wang, A. Tankasala, L. C. L. Hollenberg, G. Klimeck, M. Y. Simmons, and R. Rahman, Highly tunable exchange in donor qubits in silicon, npj Quantum Inf. **2**, 16008 (2016).

[19] M. T. Madzik, S. Asaad, A. Youssry, B. Joecker, K. M. Rudinger, E. Nielsen, K. C. Young, T. J. Proctor, A. D. Baczewski, A. Laucht *et al.*, Precision tomography of a three-qubit donor quantum processor in silicon, Nature (London) **601**, 348 (2022).

[20] L. Fricke, S. J. Hile, L. Kranz, Y. Chung, Y. He, P. Pakkiam, M. G. House, J. G. Keizer, and M. Y. Simmons, Coherent control of a donor-molecule electron spin qubit in silicon, Nat. Commun. **12**, 3323 (2021).

[21] A. M. Tyryshkin, S. Tojo, J. J. L. Morton, H. Riemann, N. V. Abrosimov, P. Becker, H.-J. Pohl, T. Schenkel, M. L. W. Thewalt, K. M. Itoh, and S. A. Lyon, Electron spin coherence exceeding seconds in high-purity silicon, Nat. Mater. **11**, 143 (2012).

[22] T. F. Watson, B. Weber, Y.-L. Hsueh, L. C. L. Hollenberg, R. Rahman, and M. Y. Simmons, Atomically engineered electron spin lifetimes of 30 s in silicon, Sci. Adv. **3**, e1602811 (2017).

[23] J. T. Muhonen, J. P. Dehollain, A. Laucht, F. E. Hudson, R. Kalra, T. Sekiguchi, K. M. Itoh, D. N. Jamieson, J. C. McCallum, A. S. Dzurak, and A. Morello, Storing quantum information for 30 seconds in a nanoelectronic device, Nat. Nanotechnol. **9**, 986 (2014).

[24] E. Prati, M. Hori, F. Guagliardo, G. Ferrari, and T. Shinada, Anderson-Mott transition in arrays of a few dopant atoms in a silicon transistor, Nat. Nanotechnol. **7**, 443 (2012).

[25] J. A. Miwa, P. Hofmann, M. Y. Simmons, and J. W. Wells, Direct Measurement of the Band Structure of a Buried Two-Dimensional Electron Gas, Phys. Rev. Lett. **110**, 136801 (2013).

[26] S. Shamim, S. Mahapatra, G. Scappucci, W. M. Klesse, M. Y. Simmons, and A. Ghosh, Spontaneous Breaking of Time-Reversal Symmetry in Strongly Interacting Two-Dimensional Electron Layers in Silicon and Germanium, Phys. Rev. Lett. **112**, 236602 (2014).

[27] E. Prati, K. Kumagai, M. Hori, and T. Shinada, Band transport across a chain of dopant sites in silicon over micron distances and high temperatures, Sci. Rep. **6**, 19704 (2016).

[28] S. P. Cooil, F. Mazzola, H. W. Klemm, G. Peschel, Y. R. Niu, A. A. Zakharov, M. Y. Simmons, T. Schmidt, D. A. Evans, J. A. Miwa, and J. W. Wells, In situ patterning of ultrasharp dopant profiles in silicon, ACS Nano **11**, 1683 (2017).

[29] B. E. Kane, A silicon-based nuclear spin quantum computer, Nature (London) **393**, 133 (1998).

[30] J. Salfi, J. A. Mol, R. Rahman, G. Klimeck, M. Y. Simmons, L. C. L. Hollenberg, and S. Rogge, Quantum simulation of the Hubbard model with dopant atoms in silicon, Nat. Commun. **7**, 11342 (2016).

[31] F. Ansaloni, A. Chatterjee, H. Bohuslavskyi, B. Bertrand, L. Hutin, M. Vinet, and F. Kuemmeth, Single-electron operations in a foundry-fabricated array of quantum dots, Nat. Commun. **11**, 6399 (2020).

[32] B. Pajot and B. Clerjaud, *Optical Absorption of Impurities and Defects in Semiconducting Crystals: Electronic Absorption of Deep Centres and Vibrational Spectra* (Springer Science & Business Media, 2012).

[33] K. E. J. Goh, F. Bussolotti, C. S. Lau, D. Kotekar-Patil, Z. E. Ooi, and J. Y. Chee, Toward valley-coupled spin qubits, Adv. Quantum Technol. **3**, 1900123 (2020).

[34] S. R. Schofield, N. J. Curson, M. Y. Simmons, F. J. Rueß, T. Hallam, L. Oberbeck, and R. G. Clark, Atomically Precise Placement of Single Dopants in Si, Phys. Rev. Lett. **91**, 136104 (2003).

[35] J. Salfi, B. Voisin, A. Tankasala, J. Bocquel, M. Usman, M. Y. Simmons, L. C. L. Hollenberg, R. Rahman, and S. Rogge, Valley Filtering in Spatial Maps of Coupling between Silicon Donors and Quantum Dots, Phys. Rev. X **8**, 031049 (2018).

[36] B. Voisin, J. Bocquel, A. Tankasala, M. Usman, J. Salfi, R. Rahman, M. Simmons, L. Hollenberg, and S. Rogge, Valley interference and spin exchange at the atomic scale in silicon, Nat. Commun. **11**, 6124 (2020).

[37] W. Kohn and J. M. Luttinger, Theory of donor states in silicon, Phys. Rev. **98**, 915 (1955).

[38] J. M. Luttinger and W. Kohn, Motion of electrons and holes in perturbed periodic fields, Phys. Rev. **97**, 869 (1955).

[39] C. Kittel and A. H. Mitchell, Theory of donor and acceptor states in silicon and germanium, Phys. Rev. **96**, 1488 (1954).

[40] A. Baldereschi and N. O. Lipari, Spherical model of shallow acceptor states in semiconductors, Phys. Rev. B **8**, 2697 (1973).

[41] K. Shindo and H. Nara, The effective mass equation for the multi-valley semiconductors, J. Phys. Soc. Jpn. **40**, 1640 (1976).

[42] A. L. Saraiva, M. J. Calderón, R. B. Capaz, X. Hu, S. Das Sarma, and B. Koiller, Intervalley coupling for interface-bound electrons in silicon: An effective mass study, Phys. Rev. B **84**, 155320 (2011).

[43] G. Giuliani and G. Vignale, *Quantum Theory of the Electron Liquid* (Cambridge University Press, 2005).

[44] A. K. Ramdas and S. Rodriguez, Spectroscopy of the solid-state analogues of the hydrogen atom: Donors and acceptors in semiconductors, Rep. Prog. Phys. **44**, 1297 (1981).

[45] A. J. Mayur, M. D. Sciacca, A. K. Ramdas, and S. Rodriguez, Redetermination of the valley-orbit (chemical) splitting of the 1s ground state of group-V donors in silicon, Phys. Rev. B **48**, 10893 (1993).

[46] J. K. Gamble, N. T. Jacobson, E. Nielsen, A. D. Baczewski, J. E. Moussa, I. Montaño, and R. P. Muller, Multivalley effective mass theory simulation of donors in silicon, Phys. Rev. B **91**, 235318 (2015).

[47] B. Koiller, X. Hu, and S. Das Sarma, Exchange in Silicon-Based Quantum Computer Architecture, Phys. Rev. Lett. **88**, 027903 (2001).

[48] C. W. J. Beenakker, Random-matrix theory of quantum transport, Rev. Mod. Phys. **69**, 731 (1997).

[49] M. Žnidarič, T. Prosen, and P. Prelovšek, Many-body localization in the Heisenberg XXZ magnet in a random field, Phys. Rev. B **77**, 064426 (2008).

[50] A. W. Sandvik, D. J. Scalapino, and P. Henelius, Quantum Monte Carlo study of the one-dimensional Hubbard model with random hopping and random potentials, Phys. Rev. B **50**, 10474 (1994).

[51] A. N. Bloch, R. B. Weisman, and C. M. Varma, Identification of a Class of Disordered One-Dimensional Conductors, Phys. Rev. Lett. **28**, 753 (1972).

[52] T. Giamarchi and B. S. Shastry, Persistent currents in a one-dimensional ring for a disordered Hubbard model, Phys. Rev. B **51**, 10915 (1995).

[53] B. Kramer, A. MacKinnon, T. Ohtsuki, and K. Slevin, Finite size scaling analysis of the Anderson transition, Int. J. Mod. Phys. B **24**, 1841 (2010).